Chinese Chemical Letters 35 (2024) 109190

Contents lists available at ScienceDirect

Chinese Chemical Letters

journal homepage: www.elsevier.com/locate/cclet

Three positive charge nonapoptotic-induced photosensitizer with excellent water solubility for tumor therapy

Zhe Li[1], Ping-Zhao Liang[1], Li Xu, Fei-Yu Yang, Tian-Bing Ren*, Lin Yuan, Xia Yin, Xiao-Bing Zhang*

State Key Laboratory of Chemo/Biosensing and Chemometrics, College of Chemistry and Chemical Engineering, Hunan University, Changsha 410082, China

ARTICLE INFO

Article history:
Received 9 August 2023
Revised 28 September 2023
Accepted 7 October 2023
Available online 14 October 2023

Keywords:
Water-soluble
Three positive charge
Photosensitizer
Nonapoptotic
Tumor therapy

ABSTRACT

Photodynamic therapy (PDT) has emerged as a significant cancer therapy option. Currently, cation-based organic small molecule aggregation-induced emission (AIE) photosensitizers (PSs) attract the wide attention of many scientists, due to improved reactive oxygen species (ROS) production after cationization. However, such PSs tend to localize only the mitochondria, limiting the death way of tumor cells (usually apoptosis) during PDT process, which may affect the therapeutic effect under some circumstances. Herein, we designed a novel water-soluble three positive charge PS, **TPAN-18F**, which could be distributed uniformly in cell cytoplasm and had distribution in different sub-organelles (mitochondria, endoplasmic reticulum, lysosome). The experimental results showed that **TPAN-18F**-based PDT process can not only disrupt mitochondrial functions (reducing ATP production and destroying mitochondrial membrane potential), but also elevate the intracellular lipid peroxides (LPOs) level, which evoke the non-apoptotic death manner of tumor cells. Further, *in vivo* studies showed that **TPAN-18F**-based PDT could effectively inhibit tumor growth. Accordingly, we believe that the construction of **TPAN-18F** is suggestive for tumor non-apoptotic therapy.

Malignant tumor is one of the diseases with the highest mortality rate in the 21st century and poses a serious threat to human health [1–4]. Therefore, the timely diagnosis and thorough treatment of malignant tumors are crucial for human health and safety. After decades of development, tumor-therapy methods (including surgical operation, phototherapy, chemotherapy and radiotherapy, *etc.*) [5–15] have made significant progress and been widely used in clinical treatment. Among various imaging techniques, fluorescence imaging has been considered as powerful tools for tumor diagnosis and therapy, due to high sensitivity, spatio-temporal resolution and low cost [16–23]. In addition, photodynamic therapy (PDT) as reliable and highly accurate tumor treatment could induce tumor cell death under light irradiation by activating photosensitizer (PS) to produce highly toxic reactive oxygen species (ROS), which has attracted increasing attention in tumor therapy [24,25]. Moreover, compared with chemotherapy, the photo-controllable characteristics of PDT could effectively reduce the side effects of the treatment process. Therefore, in recent years, PDT based on organic fluorescence molecules has emerged as a promising cancer treatment.

Phthalocyanines and porphyrins are the most widely investigated PSs, which have already been utilized in the clinic [26,27]. However, due to π-π stacking interactions from large aromatic ring system of molecular structure, these PSs usually aggregate in the water environment. This would cause low fluorescence intensity as well as terrible PDT efficiency, result from the aggregation-caused quenching (ACQ) effect [28]. In order to solve such problems, scientists have attempted to build PSs with the aggregation-induced emission (AIE) properties and improve their water solubility by introducing positive charges [29–34]. Delightingly, such cationization-based AIE PSs have evidently enhanced ROS generating ability (δEst is significantly reduced, which is conducive for ROS production) [28,35], and achieved impressive achievement in tumor therapy. Unfortunately, due to molecular structure with only single positive charge, such PSs could often only be localized in the mitochondria of tumor cells (Fig. 1a) [30,34–36], restricting the death way of tumor cells (usually apoptosis) during PDT process, which may affect the effectiveness of tumor treatment under some circumstances. As a result, it is still valuable for developing novel water-soluble AIE PSs to break through the limitations of mitochondrial localization.

* Corresponding authors.
E-mail addresses: rentianbing@hnu.edu.cn (T.-B. Ren), xbzhang@hnu.edu.cn (X.-B. Zhang).
[1] These authors contributed equally to this work.

https://doi.org/10.1016/j.cclet.2023.109190
1001-8417/

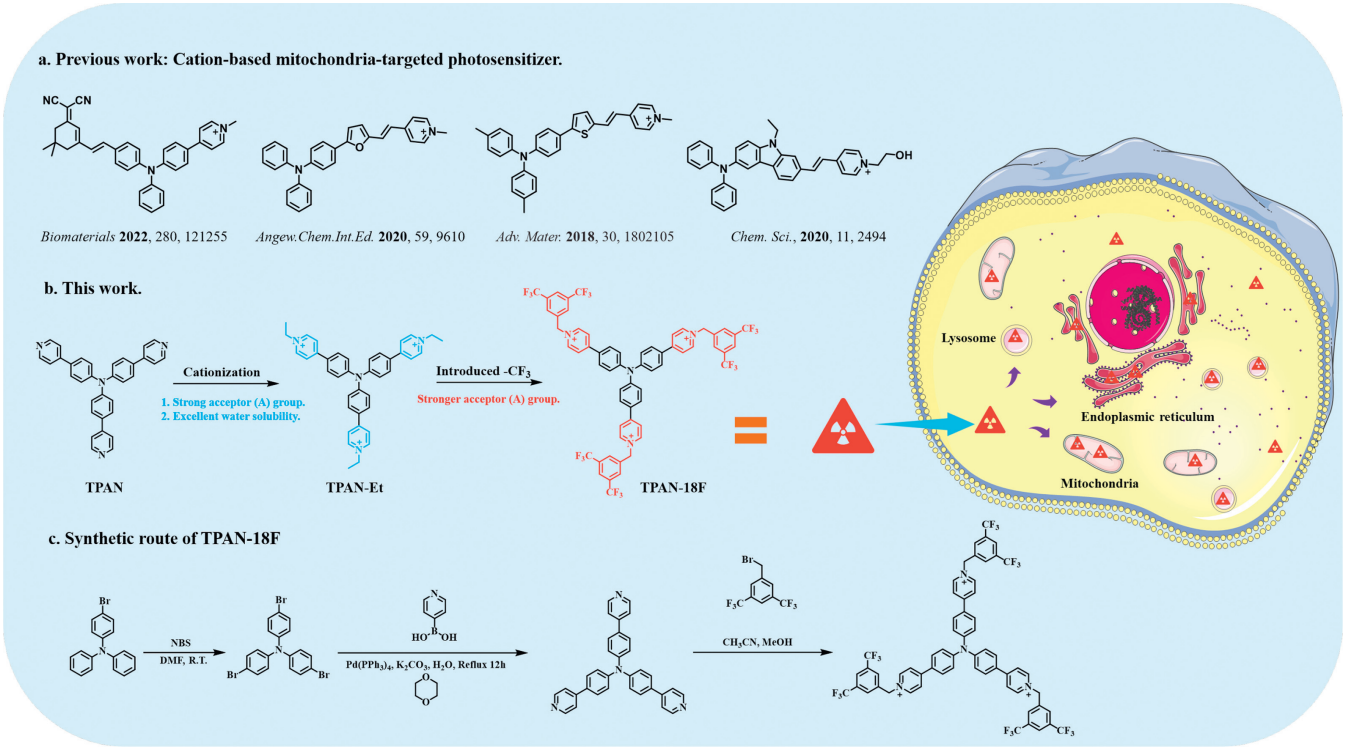

Fig. 1. (a) Previous work: Cation-based mitochondria-targeted PSs. (b) This work. (c) Synthetic route of **TPAN-18F**.

Herein, we designed a water-soluble three positive charge AIE PS (**TPAN-18F**) for tumor therapy. The experimental results showed that, **TPAN-18F** had good photosensitivity activity. Of note, **TPAN-18F** was distributed uniformly in cell cytoplasm, and had distribution in different sub-organelles (mitochondria, endoplasmic reticulum, lysosome). Due to such distribution characters, **TPAN-18F**-based PDT process can not only disrupt mitochondrial functions (reducing ATP production and destroying mitochondrial membrane potential), but also elevate the intracellular lipid peroxides (LPOs) level. On the basis, as expected, **TPAN-18F** could effectively initiate nonapoptotic cell death, as observed in cell morphology after light irradiation. Subsequent *in vivo* studies showed that the tumor growth was inhibited obviously by **TPAN-18F**-based PDT. Therefore, we are optimistic that such novel water-soluble three positive charge AIE PS are enlightening for tumor therapy.

Currently, triphenylamine-based organic AIE PSs had made many important achievements for cancer treatment (Fig. 1a). Among them, cationization-triphenylamine (with single positive charge) could effectively improve water solubility of organic compounds [29–34], further, it has been reported that appropriate introduction of positive charge could increase ROS production [28,35]. Considering that such PSs could often only be localized in the mitochondria of tumor cells [30,34-36], it would limit the death way of tumor cells (usually apoptosis) during PDT process, which may affect the effectiveness of tumor treatment under some circumstances [24]. On the basis, in order to break the single positive charge limitations and further increase water solubility, we tried to construct multi-charge PSs. As shown in Fig. 1b, by introducing ethyl to pyridine N, three-positive-charge molecule (**TPAN-Et**) can be obtained. Finally, to further increase the photosensitivity, we intend to modify **TPAN-Et** to form **TPAN-18F** by introduction six trifluoromethyl. According to previous literature, promoting intersystem crossing (ISC) from S_1 to T_1 is conducive to enhancing the photosensitization efficiency of PSs by increasing the spin-orbit coupling (SOC) and decreasing the δEST (the energy gap between S_1 state and T_1 state) based on the perturbation theory and Marcus semiclassical method [28,37]. In addition, the introduction of positive charge generally does not cause changes in SOC. Considering it, we speculated that the improvement of **TPAN-18F** was related to the change in δEST. To prove the feasibility of such option, we took advantage of density functional theory (DFT) to compute the orbital energy levels of **TPAN**, **TPAN-Et** and **TPAN-18F** (at the B3LYP/6–31G). As shown in Fig. S1 (Supporting information), the highest occupied molecular orbital (HOMO) and lowest unoccupied molecular orbital (LUMO) of **TPAN**, are distributed on the whole molecule with the poor separation. On the contrary, **TPAN-Et** and **TPAN-18F** with positive charges, changes electronic cloud distribution evidently, which produces obvious separation. Generally, the significant HOMO-LUMO separation would result in small δEs_1t_1, thus **TPAN-Et** ($\delta Es_1t_1 = 0.3702$ eV) has superior photosensitivity compared to **TPAN** ($\delta Es_1t_1 = 0.6907$ eV). Moreover, due to addition of multi-trifluoromethyl, intramolecular charge transfer (ICT) effect of **TPAN-18F** is further enhanced, which improve photosensitivity activity of **TPAN-18F** ($\delta Es_1t_1 = 0.3460$ eV). Therefore, such calculation results validate the feasibility of our above modification strategy, and we subsequently synthesized **TPAN**, **TPAN-Et** and **TPAN-18F**. The corresponding synthesis steps were shown in Fig. 1c and Scheme S1 (Supporting information), respectively. The chemical structures were characterized by matrix-assisted laser desorption/ionization time of flight mass spectrometry (MALDI-TOF MS), ^{1}H, ^{13}C nuclear magnetic resonance (NMR) and ^{19}F NMR.

The spectroscopic properties were investigated by ultraviolet–visible (UV–vis) and photoluminescence (PL) spectroscopy. In order to ensure the complete dissolution of the above compounds, we first chose dimethyl sulfoxide (DMSO) as the solvent for testing. As shown in Figs. 2a and b, the absorption and emission peaks of **TPAN** were 360 and 460 nm, respectively. Further, as expected, wavelength of **TPAN-**Et ($\lambda_{ab}/\lambda_{em} = 430/600$ nm) and **TPAN-18F** ($\lambda_{ab}/\lambda_{em} = 440/610$ nm) redshifted to visible region, which was attributed to the significant increase in ICT effects after cation-

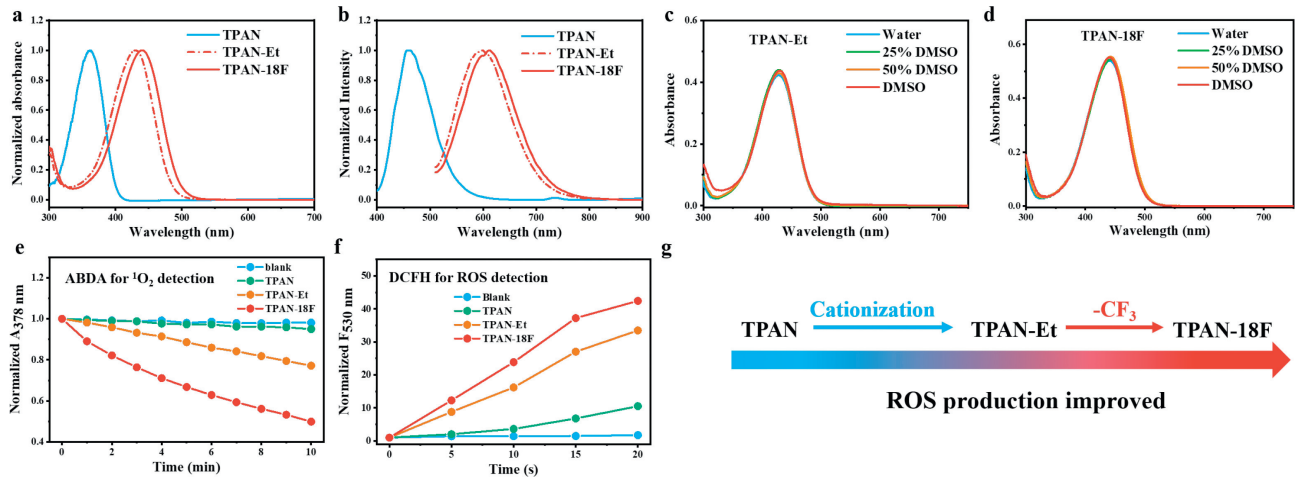

Fig. 2. Normalized absorbance (a) and fluorescence (b) spectrum of **TPAN**, **TPAN-Et** and **TPAN-18F** in DMSO. $\lambda_{ex} = 365$ nm for **TPAN**, $\lambda_{ex} = 488$ nm for **TPAN-Et** and **TPAN-18F**. (c) Absorbance of 20 μmol/L **TPAN-Et** in different solvents. (d) Absorbance of 20 μmol/L **TPAN-18F** in different solvents. (e) Time-course plots of ABDA decomposition *versus* irradiation time at $A_{378\ nm}$, $A_{378\ nm}$ represents the normalized absorbance at 378 nm. ABDA for $^1O_2$ detection. [PSs] = 5 μmol/L and [ABDA] = 75 μmol/L. (f) Time-course plots of DCFH decomposition *versus* irradiation time at $F_{530\ nm}$, $F_{530\ nm}$ represents the normalized fluorescence intensity at 530 nm. DCFH for ROS detection. [PSs] = 5 μmol/L and [DCFH] = 75 μmol/L. White light irradiation (85 mW/cm^2). (g) Schematic diagram of changes in photosensitivity of **TPAN**, **TPAN-Et** and **TPAN-18F** after modification.

ization and addition of multi-trifluoromethyl. Subsequently, in order to explore the water solubility of **TPAN-Et** and **TPAN-18F**, we tested the absorption spectrums in aqueous solutions with different DMSO content. As shown in Figs. 2c and d, **TPAN-Et** and **TPAN-18F** exhibited almost identical absorption spectra in different aqueous solutions, which indicated that they had excellent water solubility. Based on it, their photosensitive properties were studied in the water environment. By using 9′,10′-anthracenediyl-bis(methylene)-dimalonic acid (ABDA) as indicators, we first tested their $^1O_2$ production capacity. As shown in Fig. 2e and Figs. S2a–d (Supporting information), companied with the progressive addition of multi charges and trifluoromethyls, **TPAN** derivates (**TPAN**, **TPAN-Et** and **TPAN-18F**) exhibited gradually enhanced $^1O_2$ generation ability, and we calculated the singlet oxygen yield ($\Phi\Delta$) of **TPAN-18F** using Rose Bengal (RB) as a reference ($\Phi\Delta = 75\%$ in water), with values 57.4% (Fig. S3 in Supporting information). Moreover, we utilized 2′,7′-dichlorodihydrofluorescein (DCFH) as total ROS indicators to further confirm their photosensitivity activity (Fig. 2f and Figs. S2e–h in Supporting information). Consistent with previous results of $^1O_2$ generation ability, ROS production capacity was becoming increasingly stronger with the increasing positive charge, in particular, **TPAN-18F** showed the highest performance of $^1O_2$ generation (Fig. 2g), which also verified DFT calculation results.

As well known, triphenylamine group is a kind of classical AIE active units. Therefore, the effect of **TPAN-18F** on the AIE properties were subsequently studied. As shown in Figs. S4b, d, f, h and j (Supporting information), as the organic phase (EtOH and THF) content increased, the fluorescence of **TPAN-18F** was significantly enhanced, resulting from restricted molecular rotation, which was typical AIE properties. As a comparative experiment, we also tested the AIE properties of **TPAN**. The experimental results showed that, TPAN had similar properties to **TPAN-18F** (Figs. S4a, c, e, g and i in Supporting information). Besides, we found that **TPAN** and **TPAN-18F** bright solid-state fluorescence (Figs. S4i and j). And we tested the particle size of **TPAN-18F** in different solvents. The experimental results showed that **TPAN-18F** can be well dissolved in the water and no nanoparticle can be detected. But in the organic phase (EtOH and THF), significant particle sizes of **TPAN-18F** were observed. These results indicated that **TPAN-18F** indeed displayed a AIE performance (Fig. S5 in Supporting information). According to the above experimental results, we then selected **TPAN-18F** to perform following experiments.

In order to investigate the intracellular properties, we first explored the intracellular distribution of **TPAN-18F**. The distribution of **TPAN-18F** in cells could be conveniently visualized by confocal laser scanning microscopy. Various sub-organelle co-localization indicators, including Hoechst 33258 (for cell nuclear), Mito-Deep Red (for mitochondria), Lyso-Red (for lysosome) and ER-Blue (for endoplasmic reticulum), were utilized for imaging after co-incubation with **TPAN-18F** in cells. As shown in Fig. 3a, **TPAN-18F** entered the living cells obviously. According to overlap images, **TPAN-18F** had a certain distribution in sub-organelles (mitochondria, lysosomes, endoplasmic reticulum) in the cytoplasm except for the cell nucleus, which meant that **TPAN-18F** had the potential to affect many different intracellular physiological processes. Different from cationization-triphenylamine PSs with single positive charge, **TPAN-18F** did not localized in the mitochondria, which may be attributed to further improvements in water solubility form addition of two positive charges. Subsequently, to assess the potential of **TPAN-18F** for tumor therapy, we tested the capability to produce ROS in intracellular environment by utilizing DCFH diacetate (DCFH-DA) as indicators. As observed in Fig. 3b, the green channel of DCFH-DA displayed palpable enhancement after white light irradiation for **TPAN-18F** treated cells, which indicated good ROS generation capacity of **TPAN-18F** in cells.

And we further evaluated the ability of **TPAN-18F** to kill tumor cells under light irradiation by live/dead staining experiments based on calcein AM/propidium iodide (PI). As observed in Fig. 3d, green fluorescence from calcein AM was shown in cells for only **TPAN-18F** group as well as only light irradiation group, which indicated their outstanding cell viability. And **TPAN-18F** treated cells with light irradiation exhibited evident red fluorescence, which confirmed that the presence of **TPAN-18F**-based PDT would kill tumor cells. In addition, we also conducted MTT assays to further evaluate cell viability (Fig. S6 in Supporting information), and the experimental results showed that **TPAN-18F** had negligible dark toxicity, which was consistent with the above results. Of note, the **TPAN-18F** incubated cells with light irradiation showed obvious bubbles on the cell membrane (Fig. 3c), which was significantly distinct from apoptosis (*e.g.*, nuclear fragmentation or cell shrinkage) [33].

In order to figure out the intrinsic reasons of this morphology, we analyzed the content of some intracellular parameters. In our cell experiments, companied with increasing concentration, **TPAN-**

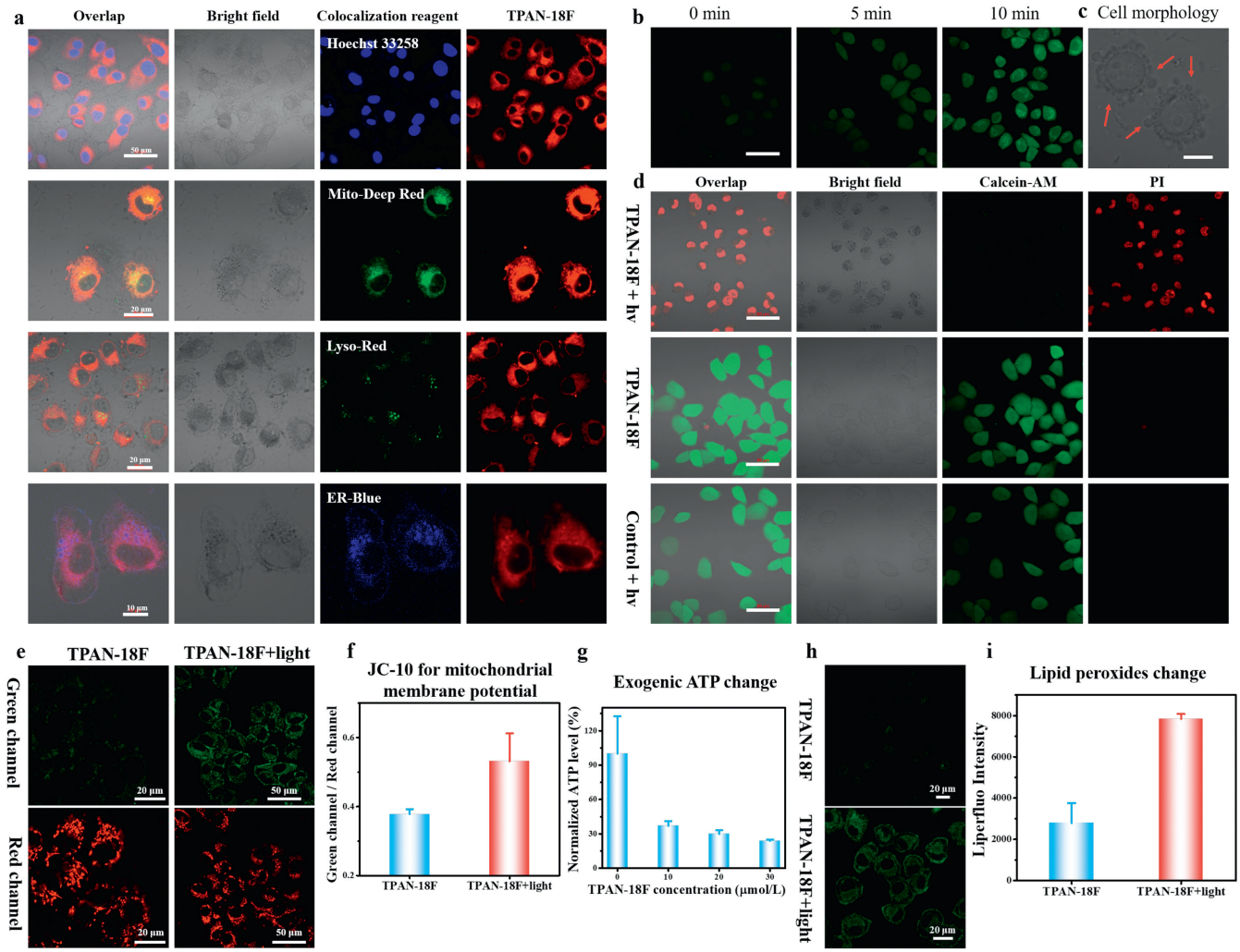

Fig. 3. (a) Fluorescence images of HeLa cells co-stained with **TPAN-18F** (5 μmol/L) and co-localization reagent (1 μmol/L). 1st column: overlap image, 2nd column: bright field, 3rd column: co-localization reagent, and 4th column: **TPAN-18F**. Hoechst 33258: $\lambda_{ex} = 405$ nm, collection channel: 425–475 nm. Mito-Deep Red: $\lambda_{ex} = 640$ nm, collection channel: 663–738 nm. Lyso-Red: $\lambda_{ex} = 561$ nm, collection channel: 663–738 nm. ER-Blue: $\lambda_{ex} = 405$ nm, collection channel: 425–475 nm. **TPAN-18F**: $\lambda_{ex} = 488$ nm, collection channel: 570–620 nm. (b) Intracellular (HeLa cells) ROS production after **TPAN-18F** (1 μmol/L) under white light irradiation (85 mW/cm^2) for different time. DCFH-DA (30 μmol/L): $\lambda_{ex} = 488$ nm, collection channel: 500–550 nm, scale bar: 50 μm. (c) The cell (HeLa cells) morphology after **TPAN-18F** (1 μmol/L) under white light irradiation (85 mW/cm^2), scale bar: 10 μm. Red arrows showed obvious bubbles. (d) Cell viability assays for HeLa cells incubated with **TPAN-18F** (5 μmol/L) in the absence and presence of light irradiation, scale bar: 50 μm. 1st column: overlap image, 2nd column: bright field, 3rd column: Calcein-AM (2 μmol/L), $\lambda_{ex} = 488$ nm, collection channel: 500–550 nm, 4th column: PI (4.5 μmol/L), $\lambda_{ex} = 561$ nm, collection channel: 570–620 nm. (e) Confocal fluorescence imaging of MMP in HeLa cells with different treatment *via* JC-10 staining, **TPAN-18F**10 μmol/L. Green channel: $\lambda_{ex} = 488$ nm, collection channel: 500–550 nm. Red channel: $\lambda_{ex} = 561$ nm, collection channel: 570–620 nm. (f) The corresponding fluorescence intensity from e. (g) Relative intercellular ATP level at different **TPAN-18F** concentrations after light irradiation. The ATP levels were detected according to the ATP content detection kit. (h) Confocal fluorescence imaging of LPO with Liperfluo under different conditions. Green channel: $\lambda_{ex} = 488$ nm, collection channel: 500–550 nm. (i) The corresponding fluorescence intensity from h. Data were displayed as mean ± standard deviation (s.d.), derived from independent biological samples ($n = 3$).

18F-based PDT was found to decrease greatly in ATP levels (Fig. 3g). According to reported literature, one of the significant features of mitochondrial damage is reducing intracellular ATP production [38]. Therefore, the mitochondrial membrane potential (MMP) during PDT was further monitored by utilizing JC-10. As shown in Figs. 3e and f, **TPAN-18F**-based PDT could severely rise mitochondrial depolarization with enhanced green channel, which further confirmed mitochondrial damage. Considering the widespread distribution of **TPAN-18F** in the cytoplasm, which may affect the function of membranes of sub-organelles, the probe Liperfluo was utilized to analyze the intracellular LPOs level. The results showed that, the green signal surrounded the nuclei indicating the increased LPOs level in cells (Figs. 3h and i), which is the important bio-marker of ferroptosis [39,40]. Therefore, based on the above results, **TPAN-18F**-based PDT could initiate non-apoptotic death manner of tumor cells.

TPAN-18F-mediated PDT was further conducted in 4T1-tumor-bearing mice. Therefore, 4T1 cancer cells were inoculated in the right leg of mice to construct the mouse tumor models (Fig. S7 in Supporting information). These 4T1-tumor-bearing mice were divided into 3 groups (that is, blank group, **TPAN-18F** group and **TPAN-18F** + light group), and monitored them every day after light irradiation.

Before the treatment, intravenous injection was conducted with 4T1 tumor-bearing mice. However, the fluorescence signal of PDT agents was not observed at the tumor region. Accordingly, in order to obtain accurate treatment results and avoid the side effects on other healthy tissues (or organs) in clinical use, *in situ* injection of PSs was selected to confirm the treatment efficiency of **TPAN-18F**. Subsequently, tumor phototherapy *in vivo* was performed by intratumorally injecting **TPAN-18F** before light irradiation. All animal experiments were conducted in accordance with

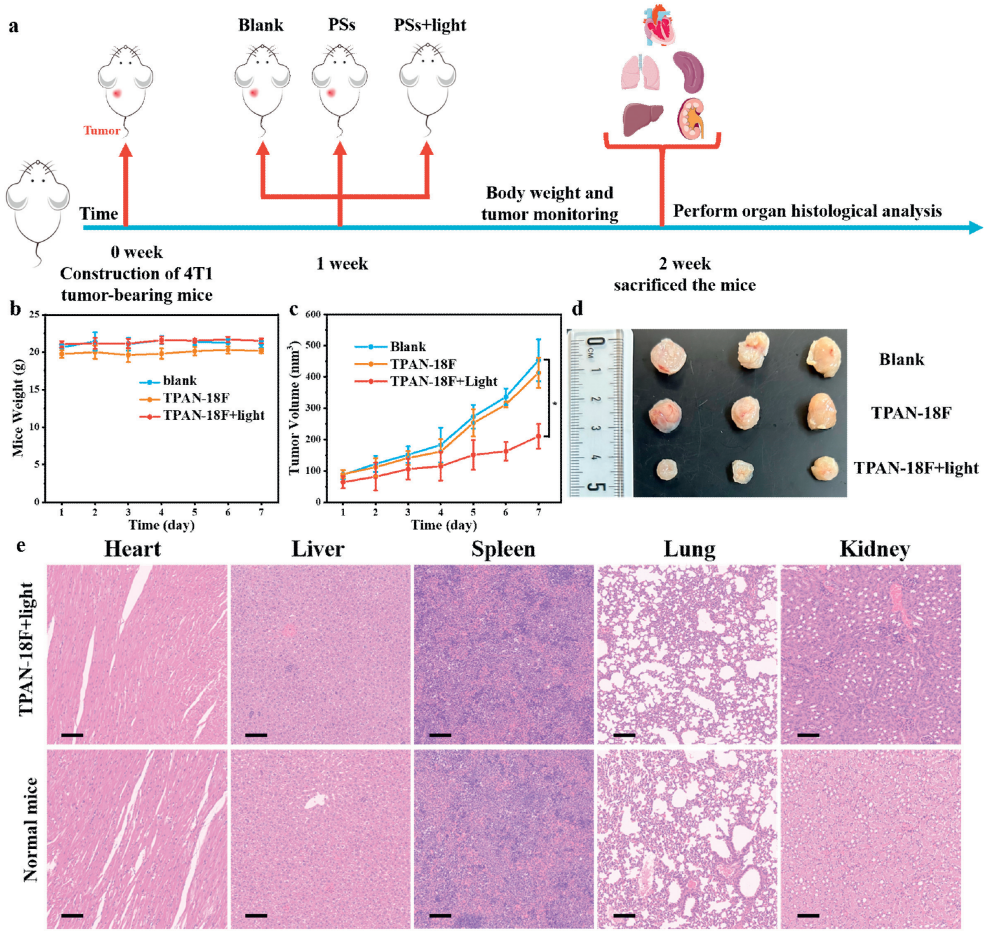

Fig. 4. (a) The relevant experiment of 4T1 tumor-bearing mice, **TPAN-18F**: 300 μmol/L (containing 5% EtOH) in PBS, 50 μL. White light irradiation (85 mW/cm^2). (b) Weight curves of experimental mice, $n = 3$. (c) Tumor growth changes of experimental mice. Data were displayed as mean ± s.d., derived from independent biological samples ($n = 3$), $^*P < 0.05$, and statistical significance was assessed through the unpaired two-sided student t-test. (d) Photos of tumor from different groups of experimental mice. (e) Histology studies of indicated mice: different organs, scale bar: 100 μm.

the Guidelines for the Care and Use of Laboratory Animals of Hunan University, and experiments were approved by the Animal Ethics Committee of the College of Biology (Hunan University). Tumor growth was monitored every day after treatment to evaluate tumor efficacy (Fig. 4a). The results showed that tumors treated with **TPAN-18F** and light irradiation were suppressed compared to blank group (Figs. 4c and d). In contrast, tumor growth in the **TPAN-18F** group only showed finite inhibited. Such results indicated that the **TPAN-18F**-mediated PDT achieved therapeutic effects. However, perhaps due to the shallow penetration of white light, the tumor did not completely ablate. In addition, to investigate the biological safety of **TPAN-18F**, experimental mice were monitored for body weight changes and processed for histological analysis of major organs. Experimental mice pre-treated with **TPAN-18F** remain stable their body weight with or without irradiation during the 7-day experimental period (Fig. 4b). According to histological analysis (hematoxylin-eosin (H.E.) results), no significant tissue damage in heart, liver, spleen, lung and kidney (Fig. 4e). Therefore, **TPAN-18F**-mediated PDT had promising biocompatibility and biosafety.

In summary, we have designed a novel water-soluble three positive charge AIE PS, **TPAN-18F**. Of note, **TPAN-18F** had excellent water solubility, whose absorption spectrum in water was coincided with DMSO. And **TPAN-18F** could enter different suborganelles (mitochondria, lysosomes, endoplasmic reticulum) in the cytoplasm which ensured that PDT could be aimed to disrupt tumor cell across the board. More importantly, **TPAN-18F**-based PDT process could not only disrupt mitochondrial functions (reducing ATP production and destroying mitochondrial membrane potential), but also elevate the intracellular LPOs level, which evoke the non-apoptotic death manner of tumor cells. This work showed that, multi-charge-based PDT reagents with huge potential, are very promising applications in tumor treatment.

Declaration of competing interest

The authors declare that they have no known competing financial interests or personal relationships that could have appeared to influence the work reported in this paper.

Acknowledgments

This work is supported by the National Science Foundation of China (No. 21890744), and the National Key R&D Program of China (No. 2019YFA0210100).

Supplementary materials

Supplementary material associated with this article can be found, in the online version, at doi:10.1016/j.cclet.2023.109190.

References

[1] H.W. Liu, L. Chen, C. Xu, et al., Chem. Soc. Rev. 47 (2018) 7140–7180.
[2] Z. Hu, C. Fang, B. Li, Z. Zhang, et al., Nat. Biomed. Eng. 4 (2019) 259–271.

[3] C. Wang, W. Fan, Z. Zhang, et al., Adv. Mater. 31 (2019) 1904329.
[4] C. Li, Y. Pang, Y. Xu, et al., Chem. Soc. Rev. 52 (2023) 4392–4442.
[5] A.B. Chagpar, R.C. Martin, L.J. Hagendoorn, C. Chao, K.M. McMasters, Am. J. Surg. 188 (2004) 399–402.
[6] M.C. Smitt, K. Horst, Ann. Surg. Oncol. 14 (2007) 1040–1044.
[7] S. Gioux, H.S. Choi, J.V. Frangioni, Mol. Imaging 9 (2010) 237–255.
[8] M. Rizzo, R. Iyengar, S.G. Gabram, et al., Ann. Surg. Oncol. 17 (2010) 228–234.
[9] A.L. Vahrmeijer, M. Hutteman, J.R. van der Vorst, C.J. van de Velde, J.V. Frangioni, Nat. Rev. Clin. Oncol. 10 (2013) 507–518.
[10] S. Liu, L. Luo, L. Zhao, et al., Nat. Commun. 12 (2021) 4014.
[11] C. Yang, G. Song, H. Yuan, et al., CCS Chem. 3 (2021) 1116–1128.
[12] Y. Xu, C. Li, J. An, et al., Sci. China Chem. 66 (2022) 155–163.
[13] J. Yuan, Q.H. Zhou, S. Xu, et al., Angew. Chem. Int. Ed. 61 (2022) e202206169.
[14] Z. Li, P.Z. Liang, L. Xu, et al., Nat. Commun. 14 (2023) 1843.
[15] H. Zhu, K. Ma, R. Ruan, et al., Chin. Chem. Lett. 35 (2024) 108536.
[16] J. Mei, N.L.C. Leung, R.T.K. Kwok, J.W.Y. Lam, B.Z. Tang, Chem. Rev. 115 (2015) 11718–11940.
[17] G. Hong, A.L. Antaris, H. Dai, Nat. Biomed. Eng. 1 (2017) 0010.
[18] P. Lu, X. Zhang, T. Ren, L. Yuan, Chin. Chem. Lett. 31 (2020) 2980–2984.
[19] S. Wang, W.X. Ren, J.T. Hou, et al., Chem. Soc. Rev. 50 (2021) 8887–8902.
[20] X. Zhang, T. Ren, F. Yang, L. Yuan, Chin. Chem. Lett. 32 (2021) 3890–3894.
[21] H. Li, H. Kim, F. Xu, et al., Chem. Soc. Rev. 51 (2022) 1795–1835.
[22] Z. Li, P.Z. Liang, T.B. Ren, L. Yuan, X.B. Zhang, Angew. Chem. Int. Ed. 62 (2023) e202305742.
[23] X. Zhang, F. Yang, T. Ren, et al., Chin. Chem. Lett. 34 (2023) 107835.
[24] W. Fan, P. Huang, X. Chen, Chem. Soc. Rev. 45 (2016) 6488–6519.
[25] X. Li, S. Lee, J. Yoon, Chem. Soc. Rev. 47 (2018) 1174–1188.
[26] J. Kou, D. Dou, L. Yang, Oncotarget 8 (2017) 81591–81603.
[27] R.C.H. Wong, P.C. Lo, D.K.P. Ng, Coord. Chem. Rev. 379 (2019) 30–46.
[28] Z. Liu, H. Zou, Z. Zhao, et al., ACS Nano 13 (2019) 11283–11293.
[29] C. Gui, E. Zhao, R.T.K. Kwok, et al., Chem. Sci. 8 (2017) 1822–1830.
[30] D. Wang, M.M.S. Lee, G. Shan, et al., Adv. Mater. 30 (2018) e1802105.
[31] D. Wang, H. Su, R.T.K. Kwok, et al., Chem. Sci. 9 (2018) 3685–3693.
[32] Y. Gao, X. Wang, X. He, et al., Adv. Funct. Mater. 29 (2019) 1902673.
[33] T. Zhang, Y. Li, Z. Zheng, et al., J. Am. Chem. Soc. 141 (2019) 5612–5616.
[34] W. Xu, M.M.S. Lee, J.J. Nie, et al., Angew. Chem. Int. Ed. 59 (2020) 9610–9616.
[35] Y. Yu, S. Wu, L. Zhang, et al., Biomaterials 280 (2022) 121255.
[36] Z. Zheng, H. Liu, S. Zhai, et al., Chem. Sci. 11 (2020) 2494–2503.
[37] S. Xu, Y. Yuan, X. Cai, et al., Chem. Sci. 6 (2015) 5824–5830.
[38] C. Jiang, X. Li, F. Pan, et al., Adv. Funct. Mater. 33 (2023) 2211698.
[39] Z. Dong, P. Liang, G. Guan, et al., Angew. Chem. Int. Ed. 61 (2022) e202206074.
[40] W. Li, S. Yin, Y. Shen, et al., J. Am. Chem. Soc. 145 (2023) 3736–3747.